Adsorption of Azobenzene on Graphene

A first-principles study

BACHELORARBEIT

zur Erlangung des akademischen Grades
Bachelor of Science
(B. Sc.)
im Fach Physik

eingereicht an der
Mathematisch-Naturwissenschaftlichen Fakultät I
Institut für Physik
Humboldt-Universität zu Berlin

von
Herr Philipp Häffner
geboren am 21.06.1990 in Karlsruhe

Erstgutachter: *Prof. Dr. Dr. hc Claudia Draxl*

Zweitgutachter: *Prof. Dr. Jürgen P. Rabe*

eingereicht am: *22. August 2014*

Acknowledgement

This work would not have been possible without the help of the research group of Prof. Dr. Dr. hc Claudia Draxl. I would like to thank in particular Caterina Cocchi for her patience and kind assistance during the whole project. The detailed explanations of Stefan Kontur and Pasquale Pavone were of great support for my Bachelor thesis.

Contents

Introduction

The aim of this work is to examine by means of first-principles calculations the electronic properties of azobenzene adsorbed on graphene. These results will be compared to those of pristine graphene. The extended π-bond network of graphene is an excellent substrate to host C-based molecules with aromatic rings. Moreover, the electronic properties of this material are very sensitive to the presence of even weakly interacting molecules. Azobenzene is, due to its switching property, a promising choice for the combination of a graphene substrate and an organic molecule. This study represents the starting step towards an understanding of the effects due to the interaction between azobenzene and graphene-based materials. In view of probable further application in electronic devices, it is of great importance to understand coupling effects on the electronic structure of such systems.

There is already a large variety of studies on the electronic properties of graphene. Among many other observed effects, small changes in the number of charge carriers of graphene lead to distinctive differences in its resistivity, due to the ambipolar electric field effect, see reference [1].

As like graphene, azobenzene is a topic of interest for recent material research. It is known that azobenzene appears in two different configurations and that it can switch between these during an isomerization [2]. The isomerization is reversible and can be induced by light irradiation [2] in a photoisomerization. More recent studies have shown that the photoisomerization of azobenzene may depend on the surface, see reference [3].

Several studies have shown that azobenzene physisorbed on graphene is a promising system for the purpose of the present work. Peimyoo et al. found charge transfer between a graphene substrate and physisorbed, functionalized azobenzene molecules [4]. The charge transfer leads to p-doping with respect to isolated graphene and shifts the Fermi energy under the Dirac crossing. Beyond that, the degree of charge transfer depends on the conformation (cis or trans) of the azobenzene derivatives.

The results presented in this work are obtained by DFT ab-initio calculations performed with the full-electron code **exciting** [5]. In this framework, a variety of different configurations of azobenzene on graphene will be investigated and compared to pristine graphene. The geometry will be regarded in terms of the bond lengths of the constituents and the separation between the molecule and the graphene substrate in its fully-relaxed configuration. The results will give information about the physisorption of the molecule on graphene. The distance between the molecule and the substrate is an indicator for the magnitude of the long-range interaction between the constituents. Additionally, there are two configurations holding the azobenzene in the same concentration and conformation, but with a slightly tilted angle towards the normal of the graphene plane. The additional configuration should allow to take into account at least small rotations of the molecule on the graphene substrate with regards to the examined properties. Furthermore, a possible torsion of

the constituents could be deduced from the calculation outcome. Finally, the band structure and density of states of the investigated system give an insight into the electronic properties and serve as an qualitative indicator for charge transfer.

Chapter 1

Theoretical Background

1.1 Basic Elements of Density Functional Theory

Density functional theory (DFT) is one of the most successful theories to describe the ground state (GS) properties of a many-body (MB) system. Such a many-body system can be described, in the non-relativistic case, by the Schrödinger equation. Its total energy depends on various physical quantities.

In order to decrease the complexity of the Schrödinger equation for crystals, several approximations were developed out of which the **Born-Oppenheimer** approximation is one of the most important. It allows to seperate the problem into a nuclei part and an electronic part which can then be solved seperately. This procedure can be regarded as a good approximation to the extent that the mass of the nuclei is by orders of magnitude larger than the mass of the electrons. Due to their higher mass the nuclei move more slowly. Within the framework of the Born-Oppenheimer approximation, the motion of the electrons is considered for fixed nuclei. In this way the MB electronic Hamiltonian becomes:

$$\left[-\frac{\hbar^2}{2m}\sum_{i=1}^{N}\bigtriangledown_i^2 \;+\; \sum_{i=1}^{N}V(\mathbf{r_i}) \;+\; \sum_{i=1}^{N}\sum_{j<i}U(\mathbf{r_i},\mathbf{r_j})\right]\psi \;=\; E_{TOT}\psi \tag{1.1}$$

what is equal to

$$\left[\hat{T} \;+\; \hat{V} \;+\; \hat{W}\right]\;\psi \;=\; E_{TOT}\psi \tag{1.2}$$

where the first term on the left-hand side defines the kinetic energy of the electron, the second describes the interaction energy between the electrons and the atomic nuclei and the third term is related to the interaction between different electrons. DFT applies the **Born-Oppenheimer** approximation whereas the electron density replaces the wave function as considered quantity. The ground state total energy is a unique functional of the electron density. Hence there is a unique mapping from the crystal Hamiltonian using MB electron wave functions to an auxiliary system of one-particle wave functions that lead to the same electron density. While doing so does not simplyfy the problem, the number of arguments needed decreases from the 3N spatial coordinates for a MB electron wave function to 3 spatial coordinates for the electron density. The electron density is composed of the wave function as follows:

$$n_0(\mathbf{r}) = N\;\int\;|\Psi_0(\mathbf{r},\mathbf{r_2},\mathbf{r}_3...\mathbf{r_N})|^2\;d\mathbf{r_2}...d\mathbf{r_N} \tag{1.3}$$

where $\Psi_0(\mathbf{r},\mathbf{r_2},\mathbf{r}_3...\mathbf{r_N})$ is the ground state wave function of an N-particle system.

1.1.1 The Hohenberg-Kohn Theorems

The theoretical foundation of DFT is given by two theorems of Hohenberg and Kohn (HK theorems). The first theorem states that the ground state energy of a non-relativistic system of interacting electrons described by the Hamiltonian as in (1.1) is a unique functional of the electron density [6]. In this framework, E_{TOT}, as computed in (1.1) can be written as:

$$E[n] \;=\; \int n(\mathbf{r})v(\mathbf{r})d^3r + F[n] \tag{1.4}$$

In equation (1.4) $v(\mathbf{r})$ is related to the external potential and $F[n]$ is decomposed as follows:

$$F[n] \;=\; T[n] \;+\; W[n] \tag{1.5}$$

$F[n]$ is a universal functional, in other words, it depends on the number of electrons only. On the contrary, $v(\mathbf{r})$ depends additionally on the specific features of the investigated system.

The second HK theorem states that the correct electron density yields the minimum E_{TOT} according to (1.4). The energy functional $E[n]$ can be minimized in order to determine both the GS total energy E_{TOT} and the GS density $n_0(\mathbf{r})$.

1.1.2 The Kohn-Sham Scheme

To put the HK theorems into action, Kohn and Sham proposed a scheme of mapping the MB problem into an auxiliary system of non-interacting electrons [7]. This set of single particle wave functions yields the same electron density as the corresponding MB wave functions. In this way, the MB problem can be mapped into a set of equations.

$$\left[-\frac{1}{2}\bigtriangledown^2 + v_{KS}\right]\psi_i \;=\; \epsilon_i\psi_i \tag{1.6}$$

The first term on the left-hand side corresponds to the kinetic energy, the second refers to the Kohn-Sham potential that, according to Kohn and Sham, is again composed of the sum of three terms.

$$v_{KS} \;=\; v_{ext} \;+\; v_{Hartree} \;+\; v_{XC} \tag{1.7}$$

The first term v_{ext} is the external potential exerted on electrons, e.g. by the nuclei. The second contribution $v_{Hartree}$ describes the interaction between the electrons due to their Hartree potential. The last term v_{XC} is the exchange correlation potential. It is the only term within the Kohn-Sham scheme that is not exactly known. A great branch of research in DFT is dedicated to finding suitable approximations for this term. This will be regarded more in detail in section (1.2).

1.2 Exchange-correlation Potential

As already mentioned, the exchange correlation functional is the only term in the Kohn-Sham equations (1.7) whose exact formulation is unknown and that therefore

determines the accuracy of the calculation. Facing this problem, there is variety of approximations to v_{XC}.

The simplest approximation is the so-called Local Density Approximation (LDA) [7], where the exchange correlation functional E_{XC} takes the following form:

$$E_{XC}^{LDA} = \int \epsilon_{XC}^{LDA}(n(\mathbf{r}))n(\mathbf{r})d^3r \tag{1.8}$$

$\epsilon_{XC}^{LDA}(n(\mathbf{r}))$ is the exchange correlation energy per particle and $n(\mathbf{r})$ the electron density. LDA is derived from the homogenous electron gas. The exchange correlation functional depends only on the value of electron density at a certain point $\mathbf{r}$ within the volume that is to be evaluated. It thus works well as far as the electron density varies slowly.

A step further in the description of the exchange correlation functional is taking into consideration not only the value of electron density, but also its first order variation. This gave rise to a new family of exchange correlation functionals following the so-called Generalized Gradient Approximation (GGA). In this framework, the functional is expressed by the electron density and the gradient of electron density:

$$E_{XC}^{GGA} = \int \epsilon_{XC}^{GGA}(n(\mathbf{r}), \bigtriangledown n(\mathbf{r}))n(\mathbf{r})d^3r \tag{1.9}$$

The first formulation of GGA was done by Langreth, David and Perdew in 1980 [8]. Later, in 1996, Perdew, Burke and Ernzerhof developed a more sophisticated form of the functional that is named after the initials of their names: **PBE** [9].

1.3 Approaches to Solve the Kohn-Sham Equations

The Kohn-Sham equations can be solved by expanding their solutions (Kohn-Sham orbitals) into a fixed basis set. For this purpose, a number of approaches has been developed in recent years. In different regions in space, the wave function has a different tendency to oscillate. In the vicinity of the atomic sites, the wave function will be prone to oscillate distinctively due to a strong Coulomb potential. Opposed to this, the shape of the wave function in the space far from the atomic sites is rather similar to that of a plane wave. To cope with the complex behavoir of crystal wave functions and therefore guarantee the accuracy of the calculation, several approaches to solve the Kohn-Sham equations have been developed. Among these, the (L)APW+lo methods, as implemented in the all-electron full-potential code **exciting**, are employed in this work [5].

1.3.1 APW - Augmented Plane Wave Method

In 1937, John Clarke Slater developed a method to describe electron wave functions [10] in crystal structures. The main concept is to subdivide the space into two types of regions. The atomic sites are surrounded by spheres (also called muffin-tin spheres, MT) and the residual space is defined as intersititial region (I), as can be seen in figure (1.1).

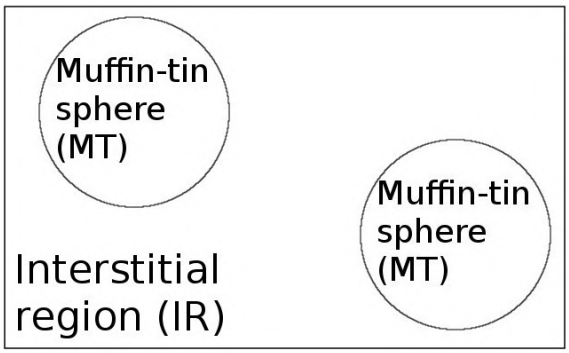

Figure 1.1: Within APW and related methods, space is subdivided into intersitial space (I) and muffin-tin spheres (MT)

The wave function is then established for each region independently. In the interstitial, it is a superposition of plane waves. Inside the spheres, the wave function is composed of the sum of the products of a radial and a spherical function:

$$\phi^{APW}_{\mathbf{G}+\mathbf{k},\epsilon(\mathbf{k})}(\mathbf{r}) \;=\; \begin{cases} \sum\limits_{l,m} A^{\mathbf{G}+\mathbf{k}}_{lm} u_l(r,\epsilon) Y_{lm}(\theta,\varphi) & \text{for } \mathbf{r} \in \text{MT}, \\ \dfrac{1}{\sqrt{\Omega}} \exp(i(\mathbf{G}+\mathbf{k})\mathbf{r}) & \mathbf{r} \in \text{I} \end{cases} \tag{1.10}$$

In this definition, $u_l(r,\epsilon)$ represents radial functions and $Y_{lm}(\theta,\varphi)$ refers to spherical functions. In addition to that, a boundary condition is introduced in order to match the basis functions of inside the muffin-tin sphere and interstitial region on the surface of each muffin-tin sphere. This then determines the coefficient $A^{\mathbf{G}+\mathbf{k}}_{lm}$. As a consequence of this, the problem of finding the electron wave functions is then transformed into finding the coefficients of the following equation:

$$\psi_{i\mathbf{k}}(\mathbf{r}) \;=\; \sum_{\mathbf{G}} c_{i(\mathbf{G}+\mathbf{k})} \phi_{\mathbf{G}+\mathbf{k},\epsilon(\mathbf{k})}(\mathbf{r}) \tag{1.11}$$

To make this equation accessible to computational analysis, one truncates the infinite sum over G. In practice, the resulting calculation parameter G_{kmax} takes to a large extent influence on the accuracy of the calculation.

The basis functions inside the muffin-tin spheres must solve the Kohn-Sham equations. As the radial function depends on energy, the latter needs to be given as a parameter. At the same time energy is the unknown and searched quantity. The problem thus becomes non-linear. The computational effort to find an energy parameter whose corresponding basis functions yield an energy eigenvalue that does not differ from the introduced energy parameter is very high. Regarding this, the APW method is not generally suitable for finding the basis functions for a system whose energy eigenvalues are not explicitly known.

1.3.2 LAPW - Linearized Augmented Plane Wave Method

Facing the non-linearity of the APW method described in the previous section, a further method has been developed to avoid the computational effort caused by this

issue. The idea is to expand the radial function with respect to energy in a Taylor series and truncate it after the linear term.

$$u_l(r,\epsilon) \;=\; u_l(r,\epsilon_l) \;+\; (\epsilon_l \;-\; \epsilon)\frac{\partial u_l}{\partial \epsilon}\bigg|_{\epsilon \;=\; \epsilon_l} + O(\epsilon_l \;-\; \epsilon)^2 \tag{1.12}$$

As a consequence of this, the introduced energy parameter does not need to be exactly equal to the eigenvalue of the regarded system. This approach is called Linearized Augmented Plane Wave Method (LAPW) and was proposed in a paper of Andersen in 1975 [11]. Its basis set can be written as:

$$\phi^{LAPW}_{\mathbf{G}+\mathbf{k},\epsilon(\mathbf{k})}(\mathbf{r}) \;=\; \begin{cases} \sum\limits_{l,m} \left[A^{\mathbf{G}+\mathbf{k}}_{lm} u_l(r,\epsilon) + B^{\mathbf{G}+\mathbf{k}}_{lm} \dot{u}_l(r,\epsilon)\right] Y_{lm}(\theta,\varphi) & \text{for } \mathbf{r} \in \mathrm{MT}, \\ \dfrac{1}{\sqrt{\Omega}} \exp(i(\mathbf{G}+\mathbf{k})\mathbf{r}) & \mathbf{r} \in \mathrm{I} \end{cases} \tag{1.13}$$

where $\dot{u}_l(r,\epsilon)$ is the derivative of the radial function with respect to energy. Within the LAPW method, there are two coefficients for each basis function within the muffin-tin sphere instead of only one as in APW. They are determined by matching the basis functions at the surface of the muffin-tin spheres in their value and first derivative. This constrain leads to an increased basis set size compared to the APW method for a preset accuracy. The basis functions thus obtained can again be superposed as described in (1.11), so as like for the APW method, the only variational parameter is $c_{\mathbf{G}}$.

1.3.3 APW + lo

Another way to avoid the nonlinear eigenvalue problem is to add local orbitals to the basis set as it is used in the APW method. This proceeding was first published by Sjöstedt, Nordström and Singh in 2000 [12]. Local orbitals are similar to the basis functions defined in the muffin-tin sphere in the framework of APW (see equation (1.10)). The difference is the fixed linearization energy used within the APW + lo method. Local orbitals can be described by:

$$\phi^{lo}_{\mathbf{G}+\mathbf{k},\epsilon_l}(\mathbf{r}) \;=\; \begin{cases} \sum\limits_{l,m} \left[A^{lo}_{lm} u_l(r,\epsilon_l) + B^{lo}_{lm} \dot{u}_l(r,\epsilon_l)\right] Y_{lm}(\theta,\phi) & \text{for } \mathbf{r} \in \mathrm{MT}, \\ 0 & \mathbf{r} \in \mathrm{I} \end{cases} \tag{1.14}$$

where the coefficients A_{lm} and B_{lm} can be determined by normalization and the boundary condition that the value of the local orbitals must be zero at the surface of the muffin-tin sphere. In this way the size of the basis set is nearly the same as in the APW method. At the same time, by introducing local orbitals, one achieves a variational freedom with regards to the radial basis functions. Due to the usage of fixed energy parameters, the problem becomes linear, as like in the LAPW method.

Chapter 2

Overview on the Investigated Systems: Graphene and Azobenzene

As previously mentioned, the aim of this work is to investigate an azobenzene molecule on graphene. This chapter gives a glimpse on some properties of these two substances.

2.1 Graphene

Graphene is a quasi two-dimensional material consisting of a single layer of carbon atoms. The latter are arranged in a hexagonal lattice giving rise to the structure shown in figure (2.1).

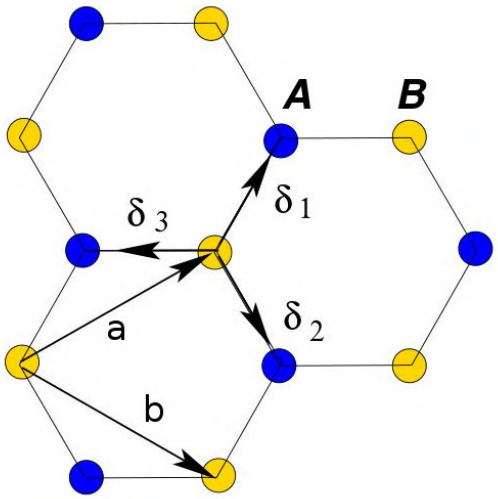

Figure 2.1: Graphene unit cell. The figure is taken from [13] and slightly modified.

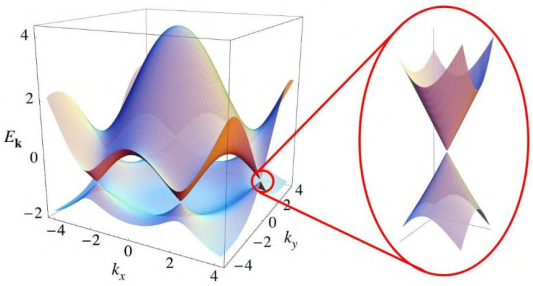

Figure 2.2: 3D Brillouin zone of graphene. The figure is taken from [13].

Figure (2.1) depicts the lattice vectors as **a** and **b**. The basis contains two atoms, A and B. Figure (2.2) shows a three-dimensional plot of the band structure of graphene. One can clearly see the Dirac cone.

Within the band structure of graphene, there is a crossing of bands at the K-point of the Brillouin zone at the Fermi energy. This circumstance leads to the definition of graphene as a zero band-gap semiconductor. In the proximity of this high-symmetry point, the bands present an almost linear dispersion what yields to an extraordinary high mobilty in the order of $\mu = 10^4 \frac{cm^2}{Vs}$ and a charge carrier speed of about $v_F \approx 10^6 \frac{m}{s}$ [14]. In 2010, the physicists A. K. Geim and K. S. Novoselov received the Noble price for having isolated and characterized graphene from bulk graphite [15]. The material they gained showed the extraordinary properties that were predicted for graphene, such as the high mobility of graphene charge carriers.

Another feature of graphene materials is the possibility to manipulate the charge carrier density up to $n = 10^{13}$ by applying a gate voltage keeping constant the high mobility [16]. Actually being close to the Fermi energy, the Dirac point of graphene can be shifted below or over the Fermi level by inducing a gate voltage or by chemical doping as well as epitaxial growth. It is a subject of recent research to induce a band gap with such manipulations and use graphene as a switch. The combination of this with the high mobility of graphene materials evokes a large interest to investigate graphene with regards to a wide field of applications in electronic devices, such as transistors [1]. An examination of the electronic properties of graphene with the help of **exciting** can be found in chapter 3.

2.2 Azobenzene

Azobenzene is a molecule composed of two phenyl groups linked by an azo group (N=N). The azobenzene molecule appears in two different conformations. In the trans phase, the molecule is flat and the phenyl rings lie on opposed sides of the azo group, see figure (2.3), left-hand side. In cis phase it is bended around the azo group leading the phenyl rings to lie on the same side of the azo group, see figure (2.3), right-hand side.

One of the most interesting features of azobenzene is its ability to switch from the trans to the cis conformation under light irradiation. This process is reversible and the cis conformation can switch back to the more stable trans conformation by irradiation or thermal relaxation. The work of Zimmermann, Chow and Paik dating back to 1957 reports on the opportunites of manipulating the conformation of azobenzene molecules. By exposure with light of different wave lengths one can achieve a highly anisomeric composition of azobenzene molecules with regards to their conformation, see reference [2]. Taking advantage of this mechanism also known as photoisomerization, azobenzene can be used in optical switching devices [17].

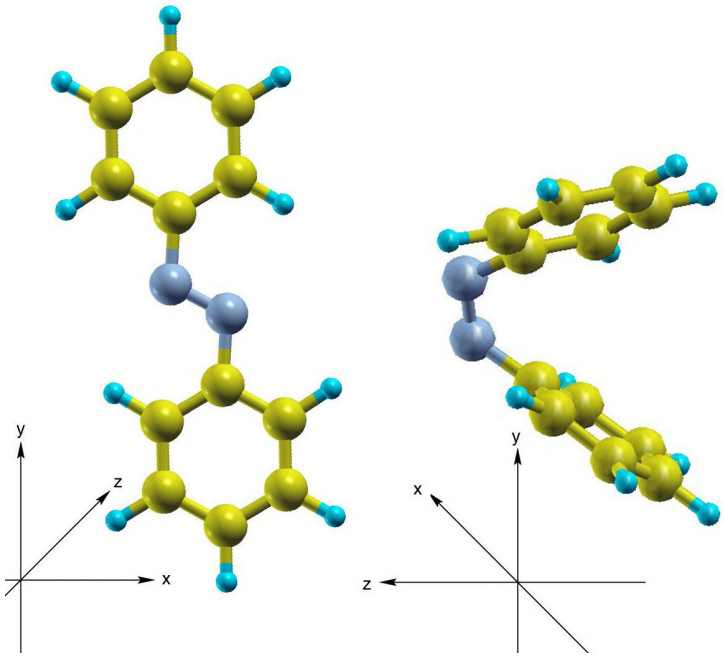

Figure 2.3: Azobenzene molecule in trans conformation (left molecule) and in cis conformation (right molecule), yellow: carbon, cyan: hydrogen, blue: nitrogen

Chapter 3

Graphene

As mentioned in section (2.1), graphene can be described by a hexagonal unit cell containing two inequivalent carbon atoms. The lattice vectors are defined as:

$$\begin{aligned} \mathbf{a} &= \sqrt{3}\, g\, \hat{\mathbf{x}} + g\hat{\mathbf{y}} \\ \mathbf{b} &= \sqrt{3}\, g\, \hat{\mathbf{x}} - g\hat{\mathbf{y}} \\ \mathbf{c} &= d\, \hat{\mathbf{z}} \end{aligned}$$

where g is the lattice parameter or, refering to figure (2.1), the magnitude of **a** or **b**. d represents the separation of two adjacent graphene layers in z-direction.

The unit cell contains two inequivalent carbon atoms at $\mathbf{p_1}$ and $\mathbf{p_2}$:

$$\begin{aligned} \mathbf{p_1} &= \mathbf{0} \\ \mathbf{p_2} &= \frac{1}{3}\,\mathbf{a} + \frac{1}{3}\,\mathbf{b} \end{aligned}$$

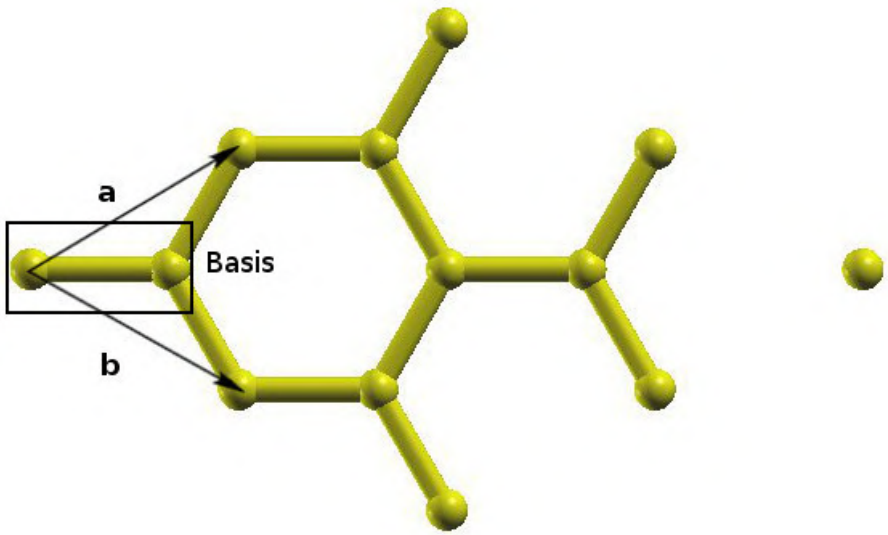

Figure 3.1: Atomic structure of graphene, **a** and **b** indicate the planar lattice vectors, the frame indicates the two atoms constituting the basis

The calculations belonging to pristine graphene are achieved in three steps. In the first, the accuracy of the obtained results is ensured by the help of convergence tests. After this, there is a volume optimization. Having found the optimized volume, one can deduce the equilibrium lattice constant from that number. In the last step and based on the previous calculations, the band structure and the density of states are calculated.

3.1 Calculation Setup and Convergence Tests

In view of performing the structure optimization and the further ground state calculation, it is necessary to determine the parameters that mostly influence the accuracy. This can be achieved by convergence tests. The convergence tests of this section refer to the sampling of k-points or k-point mesh (called **ngridk** in exciting) and the cutoff of the basis set size (called **rgkmax** in exciting). In addition to that, since graphene is a two-dimensional structure, it is necessary to determine a suitable amount of vaccum normal to the graphene planes in order to avoid unphysical interactions between the replicas.

The dimensionless parameter **rgkmax** is linked to G_{kmax}, see paragraph (1.3.1), by the relation

$$rgkmax \;=\; min(R_{MT})\; G_{kmax} \tag{3.1}$$

where R_{MT} stands for the radius of the muffin-tin sphere (MT). As already mentioned, G_{kmax} refers to the cut-off wave vector. It hence is equal to the number of wave functions used to describe the system. The value of **ngridk** gives the sampling mesh used for the integration in the Brillouin zone. The denser the k-point mesh the more accurate one can describe, for example, the dispersion in the resulting band structure. For all convergence tests within this work, the LDA exchange functional is used as implemented in the scheme of Perdew and Wang (LDA_PW) [18].

In a first test, **ngridk** $= x \times x \times 1$ is varied from x = 8 to 40 in steps of 4 keeping **rgkmax** fixed at 6. The first two components of **ngridk** can be set equal due to the symmetry of the corresponding reciprocal lattice vectors. The third component is set equal to 1, because k_z is the direction normal to the graphene plane. As the muffin tin radius of the carbon atoms for the considered system is equal to 1.3, one can see that $G_{kmax} \;\approx\; 4.62$.

Figure (3.2) shows a different convergence behavoir in dependance on the **ngridk** value being divisible by three or not. If divisible by three, sampling points are located at the Dirac cone at the K-point in the Brillouin zone. In this case, the obtained energy is higher than for a similar k-mesh that is not divisible by three. However, comparing only the total energies that are yielded using a k-mesh that is divisible by three shows as well a convergence. On the contrary, the total energies that are achieved with a k-mesh not divisible by three show a saturation in the limits of less than $\Delta E \;=\; 0.02\; mHa/atom$ for a **ngridk** $= 32 \times 32 \times 1$.

In the second test **rgkmax** was varied from 3 to 7 ($G_{kmax} \;\approx\; 2.3$ and $G_{kmax} \;\approx\; 5.4$, respectively) using the converged k-mesh of $32 \times 32 \times 1$. Figure (3.3) depicts the second test. One can see that E_{TOT} decreases continously for increasing **rgkmax** and that the differences in E_{TOT} between two subsequent values of **rgkmax** decrease as well for increasing **rgkmax**. The curve approaches a saturation. As to get a result that is converged to the order of mHa, it is necessary choose a **rgkmax** of at least

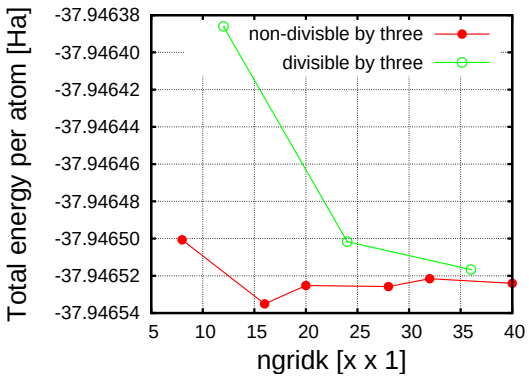

Figure 3.2: Test 1: Total energy per atom varying ngridk while rgkmax=6

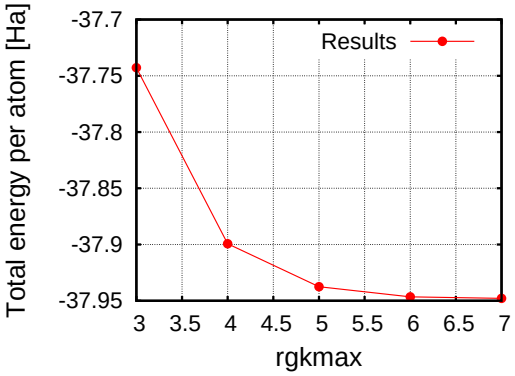

Figure 3.3: Test 2: Total energy per atom varying rgkmax from 3 to 7 while ngridk=[32 32 1]

six. Regarding the scale of the convergence test for **rgkmax** and **ngridk** it becomes clear that **rgkmax** has a much larger influence on the correctness of the obtained total energies than **ngridk**. To conclude the convergence calculations for the k-mesh and the basis set size cutoff, one can define a convergence point for the graphene sheet as follows:

$$\{\mathbf{rgkmax}, \mathbf{ngridk}\}_{Graphene} \;=\; \{6,\, 32 \times 32 \times 1\}$$

To examine the influence of the vacuum between the graphene layers, the magnitude of the lattice vector **c** normal to the graphene plane is varied from 5 Å to 17 Å. Doing so tunes the vacuum between two adjacent replica graphene planes. The total energy of each configuration was calculated. The results can be seen in figure (3.4).

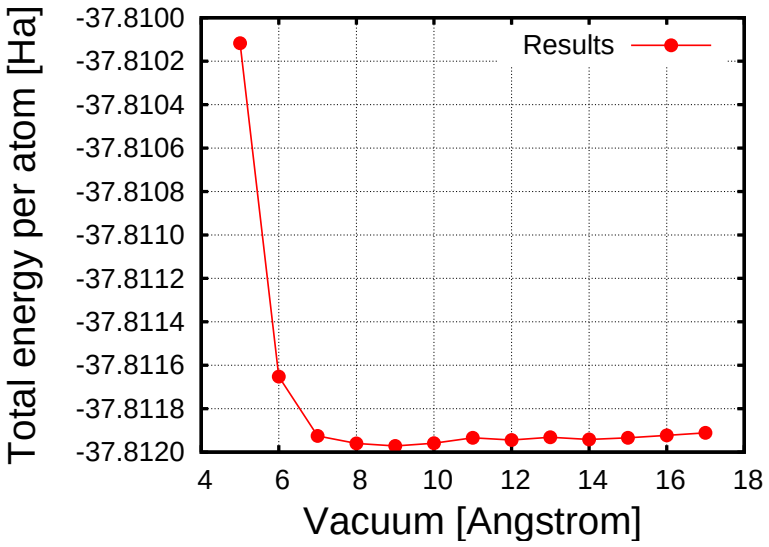

Figure 3.4: Dependency of E_{TOT} on the vacuum normal to the graphene plane. The size of the vacuum is given by the magnitude of the lattice vector **c**.

If $|\mathbf{c}|$ is smaller than 8 Å, there will be a distinctive interaction between the graphene layer replica, as can be seen in the changing of E_{TOT} in figure (3.4).

For graphene layer separations of more than 10 Å, the resulting E_{TOT} should be saturated within the order of 0.1 mHa. The influence of vacuum on E_{TOT} should then be negligible.

3.2 Results: Volume Optimization

Before examining the electronic structure of graphene, a volume optimization of the unit cell is needed. Using the same unit cell and the convergence parameters as indicated in paragraph (3.1), the lateral lattice vectors are enlarged or shortened, while the lattice vector **c**, pointing in the direction of the vacuum, is kept fixed at 19.13 b (≈ 10.12 Å). For each unit cell varied in this way, E_{TOT} was calculated. There are 18 unit cells that differ in their volume in a range of $V_1 = 336.3\ b^3$ to $V_{18} = 379.2\ b^3$. The volumes correspond to carbon atom separations of $d_C^1 \approx 2.6\ b$ and $d_C^{18} \approx 2.76\ b$, so the range between them includes the in-plane carbon atom separation of bulk graphite ($d_C^{Graphite} \approx 2.68$). For comparison, these calculations were performed with two different exchange correlation functionals, **LDA_PW** and **GGA_PBE_SOL**. The latter functional was developed by Perdew et al in 2008, see reference [19]. One may analyse the results with the help of a Taylor expansion of the total energy with respect to the volume of the supercell which truncates at third order. The function can be developed at the minimum volume V_0.

$$E(V) = E_0 + \beta \cdot (V - V_0)^2 + \theta \cdot (V - V_0)^3 + O((V - V_0)^4) \tag{3.2}$$

As can be seen in reference [20], (p.37 cf) one can neglect the linear term in the expansion as a consequence of the condition of equilibrium.

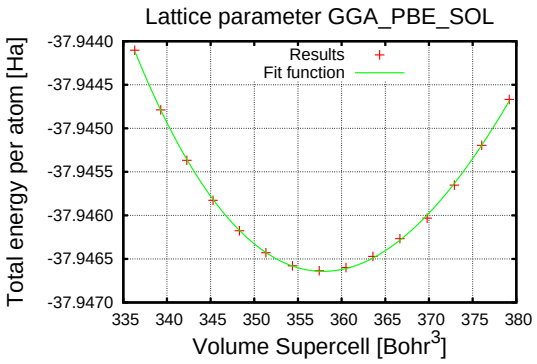

Figure 3.5: Total energy in dependance of the volume of the supercell with GGA_PBE_SOL.

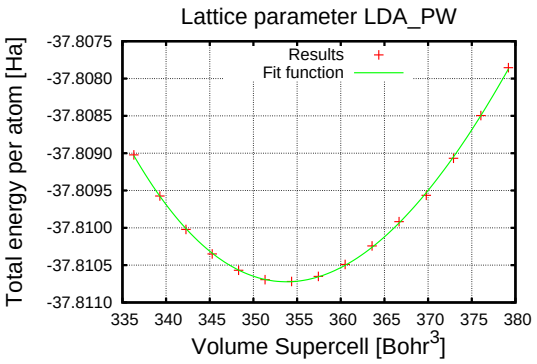

Figure 3.6: Total energy in dependance of the volume of the supercell with LDA_PW.

Both figures (3.5) and (3.6) show a minimum in E_{TOT} for an optimized unit cell volume V_0. The fit results obtained using the function (3.2) are presented in the tables below.

Table 3.1: Determined fit parameters for GGA_PBE_SOL.

Fit parameter	**Value**	**Asymptotic Standard Error**
E_0 [Ha]	-37.9466	7E-06
β [Ha/b^6]	4.87E-06	3E-08
V_0 [b^3]	357.883	0.08
θ [Ha/b^9]	-2.6E-08	3E-09

Table 3.2: Determined fit parameters for LDA_PW.

Fit parameter	**Value**	**Asymptotic Standard Error**
E_0 [Ha]	-37.8107	7E-06
β [Ha/b^6]	5.08E-06	4E-08
V_0 [b^3]	353.79	0.07
θ [Ha/b^9]	-2.5E-08	2E-09

The calculation using the GGA functional resulted in a minimum E_{TOT} that is by $\Delta E \approx 0.14\ Ha$ larger than the minimum E_{TOT} obtained with the help of the LDA functional. The optimized unit cell volume is larger by $\Delta V_0 \approx 4.1\ b^3$ when using the GGA functional instead of LDA.

The relation between the volume of the supercell and the carbon atom distance of graphene can be reckoned by using the formula of the parallelepipedal, where **a**, **b** and **c** are the lattice vectors of the supercell.

$$V = \mathbf{a}\ (\mathbf{b} \times \mathbf{c})$$

This is, due to cyclic permutation, equal to

$$V = \mathbf{c}\ (\mathbf{a} \times \mathbf{b})$$

Since there is no z-component assigned to neither **a** nor **b**, their cross product is orientated in z-direction and therefore parallel to **c**. The lattice vectors **a** and **b** are symmetric in terms of their magnitudes, so that

$$|\mathbf{a}| = |\mathbf{b}|$$

must hold. Furthermore these vectors span an angle of $\theta = 60°$ so that the formula for the supercell volume can be expressed as

$$V = |\mathbf{a}|^2\ |\mathbf{c}|\ sin(60°) \tag{3.3}$$

what gives the means to estimate the magnitude of **a** out of the volume of the supercell. $|\mathbf{a}|$ can be identified as the lattice constant. It is related to the carbon atom distance d_C by

$$d_C = \frac{|\mathbf{a}|}{\sqrt{3}} \tag{3.4}$$

so that one can deduce the carbon atom distance from the supercell volume by use of

$$d_C = \sqrt{\frac{V}{3\ sin(60°)\ |\mathbf{c}|}} \tag{3.5}$$

The fit results yield a carbon atom separation of

$$d_C^{GGA\_PBE\_SOL} = (2.684 \pm 0.004)\ b$$
$$d_C^{LDA\_PW} = (2.668 \pm 0.007)\ b$$

The value of the carbon atom distance found in literature is

$$d_C^1 = 2.68\ b\ [13]$$
$$d_C^2 = (2.6 \pm 0.2)\ b\ [21]$$

d_C^1 was computed using the tight-binding method and presented in [13], d_C^2 is an experimental value from [21]. Both computed values agree well with the theoretical carbon atom distance and are also in the uncertainty range of the experimental result. As a starting point, **LDA_PW** will be used for all further calculations done in this work.

3.3 Results: Electronic Properties

In order to examine the electronic properties of graphene, a distinct ground state calculation was performed using the optimized lattice parameter pertaining to the **LDA_PW** exchange correlation potential (see section (3.2)). Figure (3.7) shows the band structure (left-hand side) and the density of states (right-hand side) of graphene. The Fermi level is set to zero.

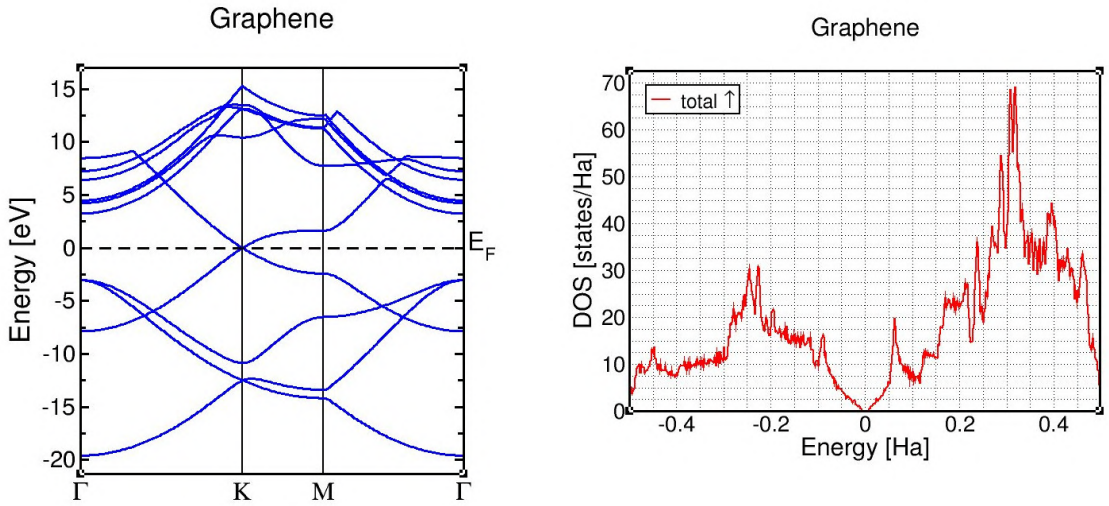

Figure 3.7: Band structure of the graphene sheet (left-hand side) and density of states (right-hand side). In both plots, the energy scale is given by $E - E_F$.

The band structure shows the characteristic Dirac cone at the K-point of the Brillouin zone. This indicates the metal-like behavoir of charge carriers in the vicinity of this high-symmetry point. The bands in the vicinity of the Dirac cone are, as expected, almost linear, leading to the high mobility of the charge carriers. The peculiar electronic properties of graphene can also be observed in the plot of the density of states in figure (3.7). As like for the band structure, the Fermi energy is set to zero. One can perceive its metallicity point at the Fermi energy.

Chapter 4

Azobenzene on Graphene

This chapter presents the results obtained for the system of an azobenzene molecule physisorbed on graphene. In order to simulate such a system, one needs to define a supercell accommodating graphene and the azobenzene molecule on top of it. The size of the included graphene sheet influences the distance between adjacent azobenzene molecules. The size of the supercell is therefore linked to the concentration of azobenzene in the system. As indicated in an experimental study of azobenzene molecules on graphene, the molecules are likely to be located close to each other, see reference [4], forming a self-assembled monolayer.

4.1 Calculation Setup

In order to simulate the different physical situations mentioned below, a set of supercells was created. The supercells differ in the size of their graphene sheet and in the conformation of their azobenzene molecule. The azobenzene molecule is arranged in a way that one of the carbon atoms of the graphene sheet is located in the center of one the phenyl rings of the molecule or vice versa, in reference to the work of Trinastic and Cheng, see reference [22]. The supercells are depicted in the following paragraphs. For better distinguishability the carbon atoms of the graphene lattice are red, the carbon atoms of the molecule are yellow, the nitrogen atoms are cyan and the hydrogen atoms are blue.

For the azobenzene in trans conformation, three supercells were established. One of them contains the trans-azobenzene and a 5x5 graphene sheet, meaning a graphene sheet consisting of 50 carbon atoms. The two supercells left contain a 6x6 graphene sheet (72 carbon atoms) and the azobenzene molecule in a slightly tilted orientations. In this way, one has a means of examining the effects of at least small changes in the orientation of the trans-azobenzene towards the graphene substrate on the measured quantities. These supercells will be refered to as trans 5x5, 6x6a and 6x6b and can be seen in figures (4.1), (4.2) and (4.3). Examining supercells with differently sized graphene sheets should give the opportunity to examine the influence of different concentrations of trans-azobenzene on the geometric and electronic properties of the system. In the 5x5 supercell containing the azobenzene in trans conformation, the hydrogen atoms of two adjacent azobenzene molecules are separated in a range of about $d = [2.2, 3.4]$ Å. The 6x6 supercell containing an azobenzene molecule in trans conformation yields molecule distances of roughly $d = [4.6, 5.7]$ Å. This reproduces experimental conditions of less interacting molecules. The initial distance between the nitrogen atom closer to the

graphene sheet and the graphene sheet is set to 3.33 Å, as in ref. [22].

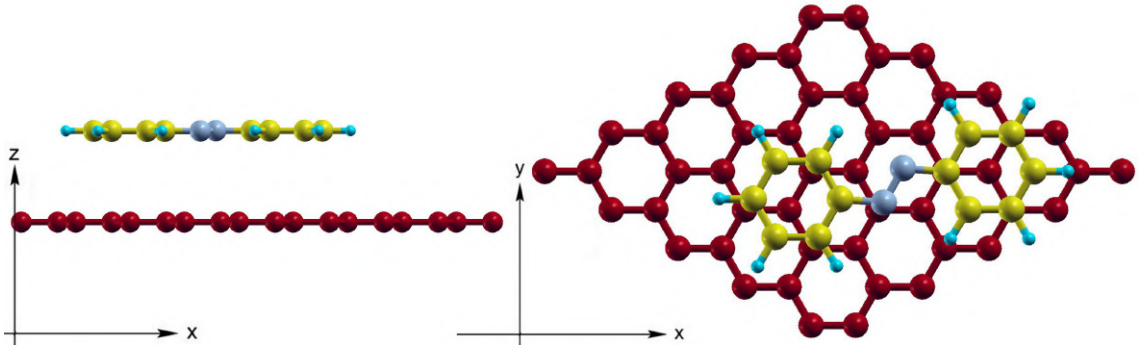

Figure 4.1: Supercell 55 trans containing a 5x5 graphene sheet plus an azobenzene molecule in trans conformation.

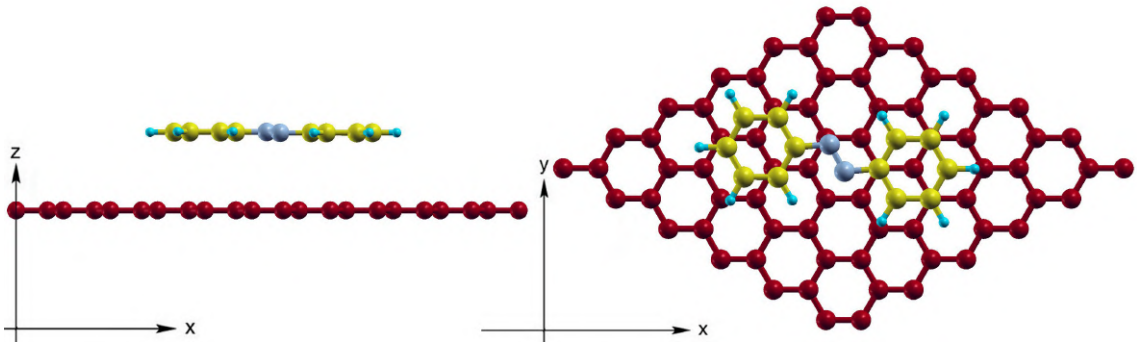

Figure 4.2: Supercell 66a trans containing a 6x6 graphene sheet plus an azobenzene molecule in trans conformation.

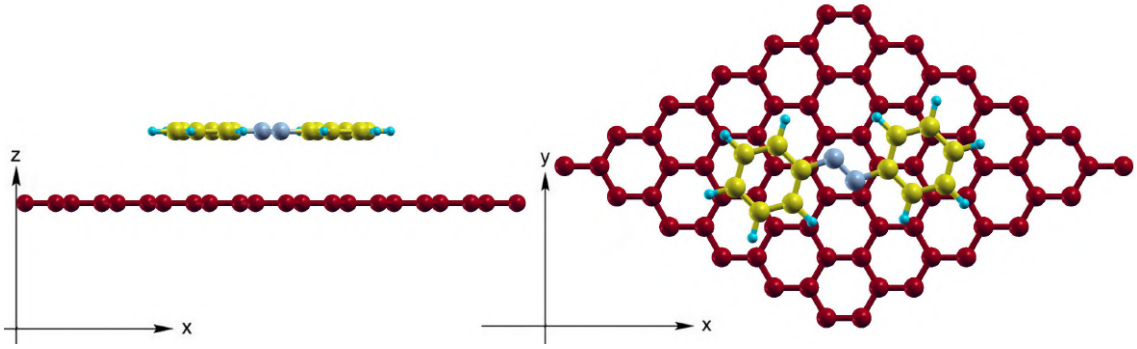

Figure 4.3: Supercell 66b trans containing a 6x6 graphene sheet plus an azobenzene molecule in trans conformation.

Concerning the cis conformation of the molecule, there is a supercell simulating a 5x5 graphene sheet and another describing a 6x6 graphene sheet. The initial distance between the nitrogen atom closer to the graphene substrate and the graphene substrate is set to 3.25 Å, again in reference to [22].

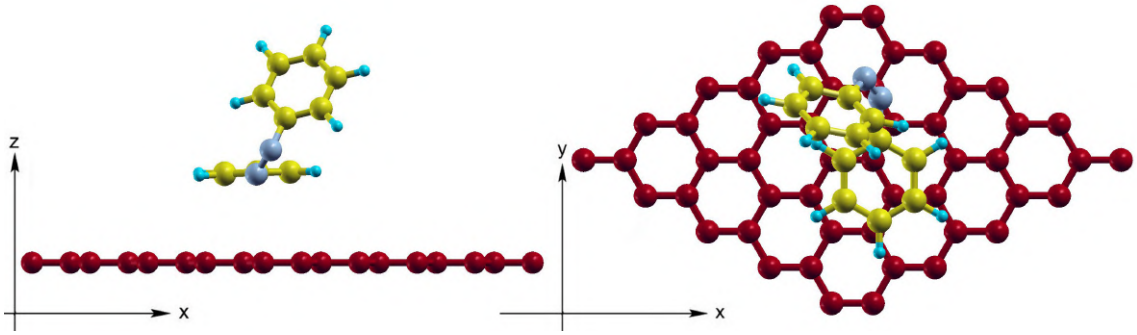

Figure 4.4: Supercell 55 cis containing a 5x5 graphene sheet plus an azobenzene molecule in cis conformation.

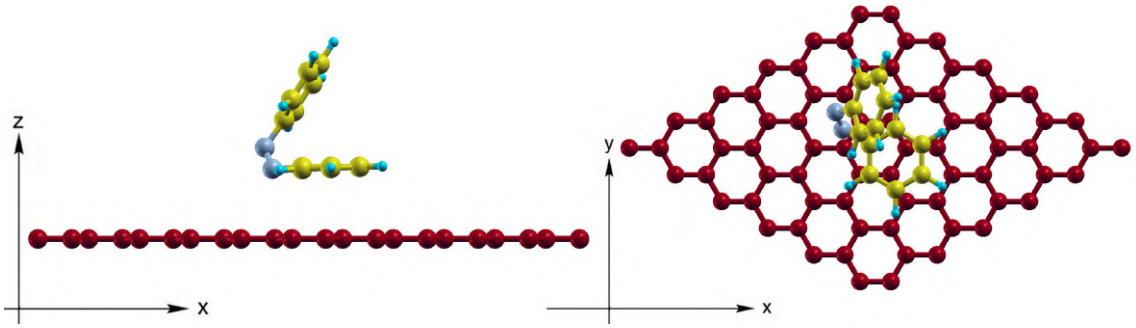

Figure 4.5: Supercell 66 cis containing a 6x6 graphene sheet plus an azobenzene molecule in cis conformation.

For all calculations of the system of azobenzene on graphene, the **LDA_PW** exchange-correlation potential was used. In a first step, a structure optimization was performed on the supercells. Within a structure optimization, the atomic positions within the supercell are varied in a way that the forces exerted on the atoms become smaller than a preset threshold F_{max}. Differing from the ground state calculation, the calculation parameters for the structure optimization were set to **rgkmax** = 2.8 (6x6 cells) and **rgkmax** = 3 (5x5 cell), corresponding to $G_{kmax} = 4$ and $G_{kmax} \approx 4.29$, respectively. The k-mesh was entirely set to **ngridk** $= 2 \times 2 \times 1$. The magnitude of the third lattice vector, that determines the distance between two adjacent graphene plane replicas, is set to 10 Å for the trans configurations and 17 Å for the supercells in cis configuration. The upper threshold for the atomic forces is set to $F_{max} = 5 \cdot 10^{-4} \frac{Ha}{Bohr}$.

In a second step, the optimized supercell was used to calculate the ground state for each system. For the ground state calculation of the supercell containing azobenzene in trans conformation, **rgkmax** is set to 3.5 (refering to a $G_{kmax} = 5$) and **ngridk** to [4 4 1]. The vacuum is increased to 15 Å.

4.2 Trans Azobenzene on Graphene

4.2.1 Geometry Optimization

As a result of the structure optimization, the distance between the graphene substrate and the azobenzene molecule was obtained. More concretely said, the distance between one of the nitrogen atoms and the graphene sheet was determined.

Table 4.1: Distances molecule - graphene of the trans supercells.

Supercell	d_{Trans} [Å]
5x5	3.19
6x6a	3.28
6x6b	3.28

The distances between the molecule and the graphene substrate decreased for all examined supercells with respect to the initial configuration ($d_{Trans}^{Initial} = 3.33$ Å). The two 6x6 supercells yield equal molecule-substrate distances. Within the 5x5 supercell, the azobenzene molecule was deplaced farer away from the initial position by $\Delta d = 0.09$ Å in comparison to the 6x6 supercells. Regarding this, on may assume that the concentration of azobenzene takes to some extent influence on the distance between graphene and the molecule.

Additionally, the bond lengths of the carbon atoms within the molecule and within the graphene sheet were measured as well as the bond length of the azo group. The results of this can be found in table (4.2).

Table 4.2: Bond lengths within the trans supercells.

Supercell	d_{N-N} [Å]	d_{C-C}^{Azo} [Å]	$d_{C-C}^{Graphene}$ [Å]
5x5	1.25	[1.38, 1.40]	1.41
6x6a	1.25	[1.38, 1.40]	1.41
6x6b	1.25	[1.38, 1.41]	1.41

The bond lengths of the two phenyl groups differ in a range of $\Delta d \approx 0.02$ Å. Beyond that, there is no evidence that the bond lengths depends on either the orientation, conformation or concentration of azobenzene. The bond lengths of graphene are not effected by the presence of the molecule. The numbers of table (4.2) show that the geometry of the constituents does not change remarkably when brought into an assembled system.

4.2.2 Electronic Properties

Using the results of the ground state calculation, the band structure of the 5x5 trans supercell was determined. In order to perceive the results of the physisorption, it seems suitable to map the band structure of the assembled system onto the one of bare graphene. Figure (4.6) depicts the band structure of bare graphene with red crosses and the band structure of the trans-azobenzene on graphene system with blue lines. One can see from figure (4.6) that the presence of the azobenzene molecule

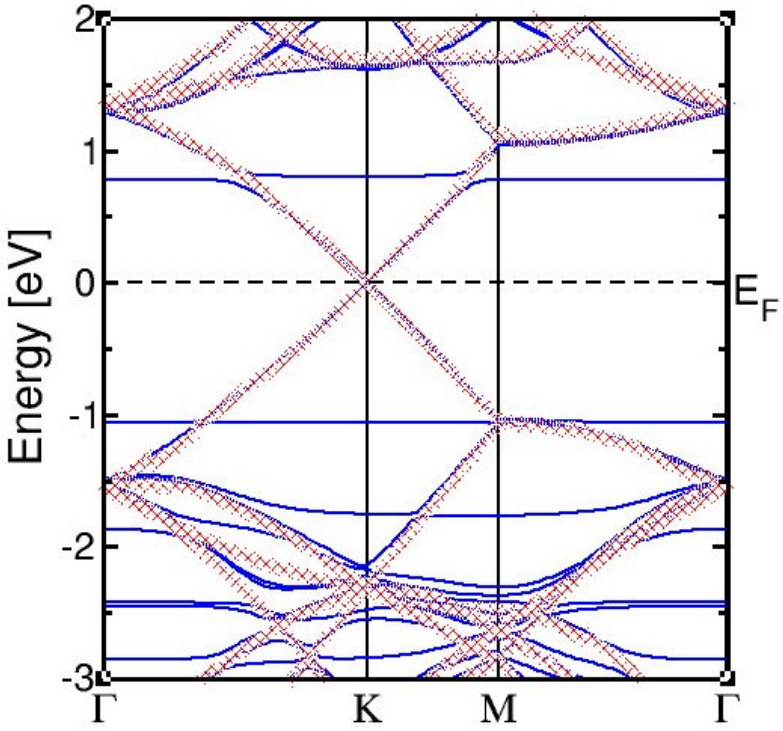

Figure 4.6: Band structures of a bare 5x5 graphene sheet (red crosses) and of the assembled trans-azobenzene on graphene system (blue lines). The energy scale is set to the Fermi energy.

adsorbed on graphene does effect severely the band structure of bare graphene. The band crossing at the metallicity point is not avoided by the presence of the molecule. The physisorbed azobenzene leads to some additional bands. Two of them are in the vicinity of the Fermi energy and flat. Between the Γ and K-point there is an anticrossing of each of the two bands due to the azobenzene and the bands of graphene that lead to the Dirac cone. This certainly is an indication for a band interaction between the two constituents. Below the Fermi energy, there are as well some additional bands stemming from the azobenzene. Bands of (isolated) molecules are usually flat, the distinctive curvature of these bands may occur as a result of the interaction between juxtaposed molecules.

In a further step, the Kohn-Sham wave functions (for brevity called wave functions in the following) of some of the bands from figure (4.6) were plotted into a scheme of the supercell, as to give an impression where the wave functions are located. This can be taken from figure (4.7). The wave functions are evaluated at the origin of the Brillouin zone. Figure (4.7) shows an issue of the anticrossing men-

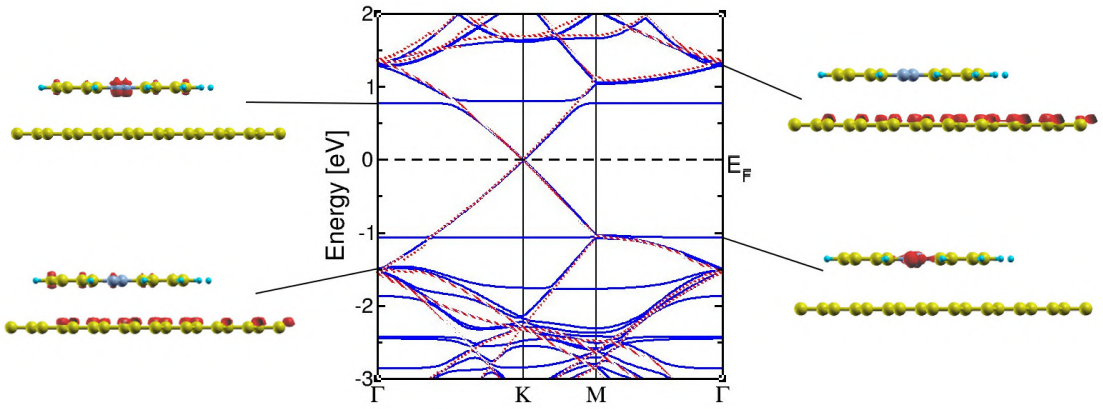

Figure 4.7: Band structures and corresponding plots of the Kohn-Sham wave functions (red). The energy scale is set to the Fermi energy.

tioned above. The band leading to the Dirac cone at the K-point interacts with one of the bands due to the molecule and therefore the Kohn-Sham wave function is, at the Γ point, entirely located at the azo-group of the molecule. The wavefunctions belonging to one of the unperturbated graphene bands are located, as expected, at the graphene. For the bands between -1 eV and -2eV, the corresponding Kohn-Sham wave functions show non-zero values both at the molecule and on the graphene substrate. This may be an indicator for a hybrid state or charge transfer between the constituents and is certainly worth being investigated in further studies.

In figure (4.8) the density of states for the trans 6x6a supercell is shown on the left-hand side and the one of the trans 6x6b supercell on the right-hand side.

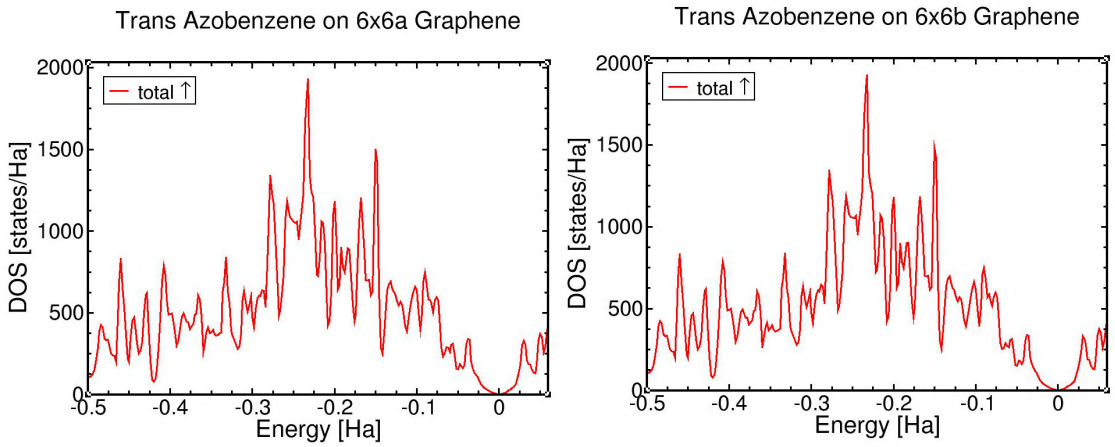

Figure 4.8: Density of states of the trans 6x6a supercell (left-hand side) and of the trans 6x6b supercell (right-hand side), the Fermi energy is set to zero.

The plots of the density of states are very similar, they show both the metallicity point at the Fermi energy. There is no perceivable influence on the density of states of the differently orientated azobenzene molecules in an equally sized supercell.

4.3 Cis Azobenzene on Graphene

4.3.1 Geometry

The structure optimization for the cis supercells was proceeded, as like for the trans supercells, with the calculation parameters mentioned above except the vacuum that was enlarged to 17 Å. Since the calculations did not finish in time, only preliminary results can be presented for the cis configuration. The distance between the molecule and the graphene was determined by measuring the distance between the nitrogen atom closer to the graphene and the graphene.

Table 4.3: Distances molecule-graphene of the cis supercells.

Supercell	d_{Cis} [Å]
5x5	3.29
6x6	3.26

The molecule-graphene distance increased while proceeding the structure optimization with respect to the initial distance ($d_{Cis}^{Initial} = 3.25$ Å). The molecule-graphene distance for the 5x5 supercell is by $d = 0.03$ Å larger than for the 6x6 supercell. As already observed for the supercell containing azobenzene in trans conformation, the concentration of azobenzene takes influence on the structure optimization: The smaller the concentration of azobenzene the less the molecule moves during the structure optimization. For the cis conformation, the determined molecule-graphene distances are more similar to the inital distance as for the trans conformation. For the azobenzene molecule being in their cis conformation, the molecule were less likely to move within the structure optimization. This issue may be due to the circumstance that one part of the azobenzene molecule is bended off the graphene sheet. The surface of the part of the azobenzene molecule that interacts with the graphene sheet thus becomes smaller and thus the interaction between graphene and azobenzene weaker.

4.3.2 Electronic Properties

For the 5x5 cis supercell a preliminary band structure was calculated as can be seen in figure (4.9). The band structure for the 5x5 cis supercell shows as well some flat

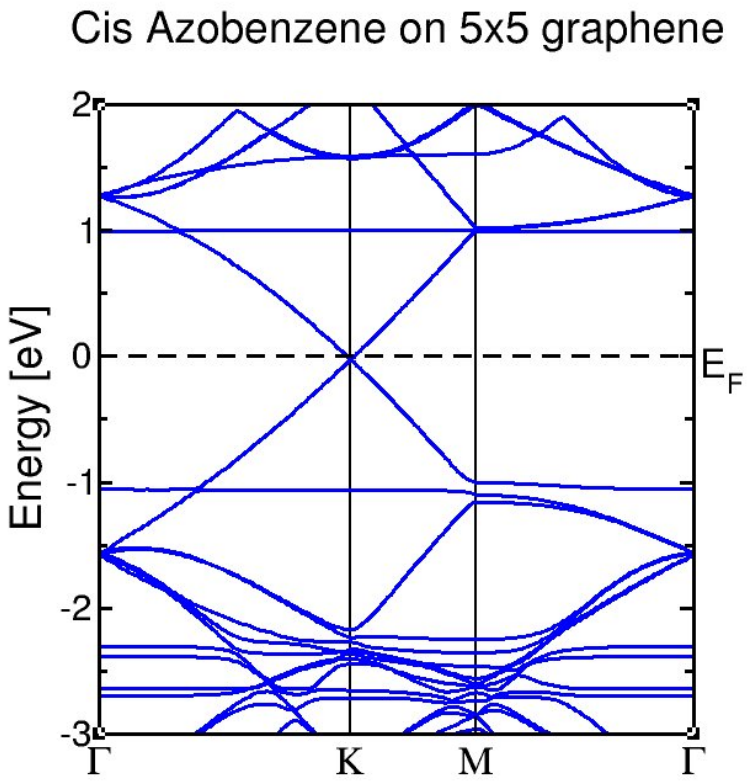

Figure 4.9: Band structure of the supercell containing a cis azobenzene and 5x5 graphene sheet, the Fermi energy is set to zero.

bands that are certainly due to the azobenzene. As like in the band structure of the trans 5x5 supercell, there are two bands due to molecular states in the vicinity of the Fermi energy. One of them is involved in an anticrossing at the M-point of the Brillouin zone, together with one of the graphene bands that constitutes the Dirac cone at the K-point. The band belonging to a molecular state far below the Fermi energy shows a noticeable curvature. This again may indicate an interaction between the molecules. In comparison to the band structure of the 5x5 trans supercell, the curvature of these band is less distinctive. This may be caused by the enlarged distance between the azobenzene molecules with respect to the trans conformation.

Conclusion

The achieved calculations point towards a couple of interesting properties of the regarded system of a physisorbed organic molecule on graphene. As already mentioned in the introduction, it is crucial to investigate the changes in geometric and electronic properties of the constituents when they are brought into an assembled system. Gathering experience in this field may allow to find a way to perform p-doping on graphene without destroying the sensitive hexagonal carbon structure that is crucial for the delocalized p-bonds and thus for the interesting electronic properties of graphene. A system that combines the electronic structure of graphene with a remarkable degree of hole doping has a distinct band gap. Such a material may give rise to investigations for new semi-conducting materials.

The performed calculations showed that azobenzene is physisorbed on a graphene substrate. This is true for both conformations of the molecule. The fully-optimized configurations of azobenzene on graphene in two different azobenzene concentrations can be used for further studies. The interaction between azobenzene and graphene does not lead to remarkable distortions in the geometry of the constituents, independent on the conformation of azobenzene. On the contrary, the conformation and concentration of azobenzene influences the distance between the graphene substrate and the molecule. Smaller concentrations lead to smaller distances for the trans conformation of azobenzene and to larger separations for the cis conformation. The differences in the substrate-molecule separation are weaker for the cis conformation. The may be induced by the larger intermolecular distances and hence weaker intermolecular interactions. An interesting result are the observed electronic band interactions of azobenzene and graphene. For both conformations, the bands caused by the molecule interact with the bands due to graphene in terms of anticrossing. The regarded anticrossing may be an indicator of the charge transfer that figures the issue of this work, as mentioned in the introduction. Further studies may investigate quantitatively the charge transfer that occurs in such a system. There is no shift in the Dirac point for the examined configurations containing the azobenzene molecule in trans conformation so that, within this work, there is no quantitative evidence for charge transfer. Opposed to that, one can perceive a small shift of the Dirac point within the preliminary band structure of the 5x5 cis system. A deeper analysis may show if this is a numerical artefact or a physical effect.

List of Figures

List of Tables

Bibliography

[1] Andre K Geim and Konstantin S Novoselov. The rise of graphene. *Nature materials*, 6(3):183–191, 2007.

[2] George Zimmerman, Lue-Yung Chow, and Un-Jin Paik. The photochemical isomerization of azobenzene1. *Journal of the American Chemical Society*, 80(14):3528–3531, 1958.

[3] Luís Duarte, Rui Fausto, and Igor Reva. Structural and spectroscopic characterization of e-and z-isomers of azobenzene. *Physical Chemistry Chemical Physics*, 2014.

[4] Namphung Peimyoo, Jiewei Li, Jingzhi Shang, Xiaonan Shen, Caiyu Qiu, Linghai Xie, Wei Huang, and Ting Yu. Photocontrolled molecular structural transition and doping in graphene. *ACS nano*, 6(10):8878–8886, 2012.

[5] Andris Gulans, Stefan Kontur, Christian Meisenbichler, Dmitrii Nabok, Pasquale Pavone, Santiago Rigamonti, Stephan Sagmeister, Ute Werner, and Claudia Draxl. exciting: a full-potential all-electron package implementing density-functional theory and many-body perturbation theory. *Journal of Physics: Condensed Matter*, 26(36):363202, 2014.

[6] Pierre Hohenberg and Walter Kohn. Inhomogeneous electron gas. *Physical review*, 136(3B):B864, 1964.

[7] Walter Kohn and Lu Jeu Sham. Self-consistent equations including exchange and correlation effects. *Physical Review*, 140(4A):A1133, 1965.

[8] David C Langreth and John P Perdew. Theory of nonuniform electronic systems. i. analysis of the gradient approximation and a generalization that works. *Physical Review B*, 21(12):5469, 1980.

[9] JP Perdew, K Burke, and M Ernzerhof. Phys rev lett 77: 3865. *Errata:(1997) Phys Rev Lett*, 78:1396, 1996.

[10] JCp Slater. Wave functions in a periodic potential. *Physical Review*, 51(10):846, 1937.

[11] O. Krogh Andersen. Linear methods in band theory. *Phys. Rev. B*, 12:3060–3083, Oct 1975.

[12] Elisabeth Sjöstedt, Lars Nordström, and DJ Singh. An alternative way of linearizing the augmented plane-wave method. *Solid state communications*, 114(1):15–20, 2000.

[13] AH Castro Neto, F Guinea, NMR Peres, Kostya S Novoselov, and Andre K Geim. The electronic properties of graphene. *Reviews of modern physics*, 81(1):109, 2009.

[14] KSA Novoselov, Andre K Geim, SVb Morozov, Da Jiang, MI Katsnelson IV Grigorieva, SV Dubonos, and AA Firsov. Two-dimensional gas of massless dirac fermions in graphene. *nature*, 438(7065):197–200, 2005.

[15] KS Novoselov, D Jiang, F Schedin, TJ Booth, VV Khotkevich, SV Morozov, and AK Geim. Two-dimensional atomic crystals. *Proceedings of the National Academy of Sciences of the United States of America*, 102(30):10451–10453, 2005.

[16] Kostya S Novoselov, Andre K Geim, SV Morozov, D Jiang, Y_ Zhang, SV Dubonos, IV Grigorieva, and AA Firsov. Electric field effect in atomically thin carbon films. *science*, 306(5696):666–669, 2004.

[17] Kevin G Yager and Christopher J Barrett. Novel photo-switching using azobenzene functional materials. *Journal of Photochemistry and Photobiology A: Chemistry*, 182(3):250–261, 2006.

[18] John P. Perdew and Yue Wang. Accurate and simple analytic representation of the electron-gas correlation energy. *Phys. Rev. B*, 45:13244–13249, Jun 1992.

[19] John P Perdew, Adrienn Ruzsinszky, Gábor I Csonka, Oleg A Vydrov, Gustavo E Scuseria, Lucian A Constantin, Xiaolan Zhou, and Kieron Burke. Restoring the density-gradient expansion for exchange in solids and surfaces. *Physical Review Letters*, 100(13):136406, 2008.

[20] David Sholl and Janice A Steckel. *Density functional theory: a practical introduction*. John Wiley & Sons, 2011.

[21] Çağlar Ö Girit, Jannik C Meyer, Rolf Erni, Marta D Rossell, C Kisielowski, Li Yang, Cheol-Hwan Park, MF Crommie, Marvin L Cohen, Steven G Louie, et al. Graphene at the edge: stability and dynamics. *science*, 323(5922):1705–1708, 2009.

[22] Jonathan Trinastic and Hai-Ping Cheng. First-principles study of multi-control doping using azobenzene adsorbed on graphene. *Bulletin of the American Physical Society*, 2014.

Selbständigkeitserklärung

Hiermit erkläre ich, dass ich die vorliegende Bachelorarbeit selbstständig und nur unter Verwendung der angegebenen Literatur und Hilfsmittel angefertigt habe. Die aus fremden Quellen direkt oder indirekt übernommenen Stellen sind als solche kenntlich gemacht. Die Arbeit wurde bisher in gleicher oder ähnlicher Form keiner anderen Prüfungsbehörde vorgelegt und auch nicht veröffentlicht.